

UNIVERSITÁ DI GENOVA

LAUREA MAGISTRALE IN INGEGNERIA MECCANICA

**On the onset of limit cycles in
models of Ansaldo's gas turbine
burners**

SULL'INSTAURARSI DI CICLI LIMITE IN MODELLI DI
BRUCIATORI DI TURBINE A GAS ANSALDO

Author:
Filippo BACCINO

Supervisor:
Prof. Alessandro BOTTARO
Co-supervisor:
Dr. Ezio COSATTO

Abstract

The present thesis makes use of COMSOL Multiphysics to deepen and widen Ansaldo Energia's approach to the matter of combustion instabilities. Both classical and original study method are taken into consideration. The importance of mean flow velocity when searching for the system's eigenfrequencies is first assessed using a given COMSOL method which solves the inhomogeneous wave equation. Subsequently, a new set of equations considering the mean flow as not negligible is implemented in COMSOL Multiphysics using its Physic Builder. Various simulations are then performed in one dimension to prove correctness of the implementation of the analytical model for the heat release in COMSOL Multiphysics and to estimate the resulting system's sensibility to inlet Mach number, initial conditions and geometry. Lastly, the implementation of our set of equation in a real combustion chamber is discussed.

La presente tesi utilizza COMSOL Multiphysics per approfondire ed allargare l'approccio di Ansaldo Energia al problema delle instabilita' di combustione. Sia metodi di studio standard sia metodi originali sono presi in considerazione. Per prima cosa, l'importanza della velocita' del flusso medio nella ricerca delle autofrequenze di un sistema viene stimata utilizzando un metodo preesistente di COMSOL che risolve l'equazione delle onde inomogenea. Di seguito un nuovo gruppo di equazioni, in cui si considera il flusso medio come non trascurabile, implementato in COMSOL Multiphysics utilizzando il Physic Builder ad esso associato. Varie simulazioni monodimensionali sono quindi condotte al fine di provare la correttezza dell'inserimento, nell'ambiente di COMSOL Multiphysics, di un modello analitico per il rilascio termico e per stimare la sensibilit del sistema risultante al numero di Mach all'ingresso, alle condizioni iniziali ed alla geometria. Infine, viene discussa l'implementazione del nostro gruppo di equazioni in una camera di combustione reale.

Contents

| | | |
|----------|---|-----------|
| 1 | Generalities on combustion instabilities | 5 |
| 1.1 | Physical explanation | 6 |
| 1.2 | Academic approach | 7 |
| 1.3 | Ansaldo Energia's approach | 8 |
| 2 | Effects of the mean flow: a literature case | 10 |
| 2.1 | Equations of thermo-acoustic | 10 |
| 2.2 | Introducing unsteady heat release and mean flow into CM's "Pressure Acoustics" module | 12 |
| 2.3 | Geometry and data | 13 |
| 2.4 | Results and observations | 15 |
| 3 | Importance of a uniform mean flow | 18 |
| 3.1 | Demonstration that the wave equation with non-uniform mean flow is non-Hermitian | 18 |
| 3.2 | Impact on our investigation | 21 |
| 4 | Thermoacoustics with mean flow | 23 |
| 4.1 | Linearization of equations | 24 |
| 4.2 | Boundary conditions | 24 |
| 4.3 | Time step and mesh size | 25 |
| 5 | Heat release model | 26 |
| 5.1 | Including the heat release model inside our equations | 32 |
| 6 | Simulations | 34 |
| 6.1 | Model I | 34 |
| 6.2 | Model II | 38 |
| 6.3 | Model III | 41 |
| 6.4 | 3D Models | 43 |
| 7 | Conclusions and future developments | 45 |

List of variables and acronyms

Latin

| | |
|-----------------------------|---|
| AE | Ansaldo Energia |
| A_f | Flame's area [m^2] |
| c | Speed of sound [$\frac{m}{s}$] |
| c_p | Specific heat at constant pressure [$\frac{J}{kg \cdot K}$] |
| c_v | Specific heat at constant volume [$\frac{J}{kg \cdot K}$] |
| CM | Comsol Multiphysics |
| FTF | Flame Transfer Function |
| H | Higher heating value [$\frac{J}{kg}$] |
| h | Enthalpy [J] |
| I | Identity matrix |
| K | Thermal conductivity [$\frac{W}{m \cdot K}$] |
| k_{eq} | Wave number [$\frac{1}{m}$] |
| L | Length [m] |
| $\mathbf{Ma} = \frac{u}{c}$ | Mach number |
| M | Mass flow [$\frac{kg}{s}$] |

| | |
|--------------|--|
| m | Molar mass $\left[\frac{kg}{mol} \right]$ |
| n | Molar concentration $\left[\frac{mol}{m^3} \right]$ |
| n^* | Order of reaction |
| p | Pressure $[Pa]$ |
| q | Heat release $\left[\frac{W}{m^3} \right]$ |
| R_s | Gas constant $\left[\frac{J}{K \cdot mol} \right]$ |
| S | Entropy $\left[\frac{J}{K} \right]$ |
| T | Temperature $[K]$ |
| \mathbf{u} | Velocity vector $\left[\frac{m}{s} \right]$ |
| v | Specific volume $\left[\frac{m^3}{kg} \right]$ |
| v_f | Flame speed $\left[\frac{m}{s} \right]$ |
| v_{fM} | Maximum flame speed $\left[\frac{m}{s} \right]$ |
| Y | Fuel mass fraction |
| z | Air molar fraction |

Greek

| | |
|------------|---|
| α | Coefficient of thermal expansion $\left[\frac{1}{K} \right]$ |
| β | Coefficient of compressibility $\left[\frac{1}{Pa} \right]$ |
| γ | Ratio of specific heats |
| δ_f | Flame thickness $[m]$ |

| | |
|----------------|---|
| λ | Eigenvalue |
| μ_0 | Dynamic viscosity [$Pa \cdot s$] |
| μ_B | Bulk viscosity [$Pa \cdot s$] |
| ρ | Density $\left[\frac{kg}{m^3} \right]$ |
| $\sigma_{i,j}$ | Stress tensor [Pa] |
| τ | Residence time [s] |
| ϕ_{10} | Viscous dissipation function $\left[\frac{W}{m^3} \right]$ |
| ω | Pulsation [Hz] |

Superscript and subscript

| | |
|---------------------|----------------------------|
| $-$ | Mean, unperturbed quantity |
| $\hat{}$ | Complex quantity |
| $'$ | Fluctuating quantity |
| 0 | Initial quantity |
| <i>critical</i> | Critical value |
| <i>inlet</i> | Considered at the inlet |
| <i>outlet</i> | Considered at the outlet |

Chapter 1

Generalities on combustion instabilities

The trend of low polluting, high performance power generators led modern gas turbine's combustor to be annular and supplied with a lean premix of gas and compressed air. This configuration, despite its advantages, promotes a dangerous interaction between heat release and pressure oscillation in combustion chambers, called humming, which sometimes leads to damages and machine failures [2]. Annular chambers were firmly established as a standard for aircraft engines since 1960's, but their advantages rapidly made them suitable also for power generators. Among the advantages, we list: highly uniform combustion, uniformity of exit temperatures and low pressure drop. One of the most important advantages for aircraft engines, compactness, is of course of minor importance for industrial combustors, except particular cases. The main drawback, which will be more evident in the following sections when discussing Ansaldo Energia's approach, is the difficulty to have meaningful test rigs in size different from the full scale. Some further requirements for those engines allows us to have a better understanding of design decisions: accessibility for maintenance and minimal shut-down time. These are some of the reasons that brought AE's annular combustion chambers to be paved with refractory bricks and equipped with multiple burners. About pollutants, the main three to be avoided are: unburned hydrocarbons (UHC), nitrogen oxides (NOx) and carbon monoxide (CO). Conventional combustors must find a compromise between the three, with the concentration of one pollutant typically rising as another one is lowered. Thus, the most common approach is to keep the mixture as lean as possible by adding air. This arrangement guarantees all the oxygen needed to complete reactions - to avoid CO and UHC formation - by contemporary lowering NOx production because of the lower temperatures achieved. Of course, lean flames also have drawbacks: risk of incomplete evaporation, auto-ignition and, last but not least, combustion instability. Given the relevance of the matter of combustion instabilities, which can compromise the machine's durability and extend shut-down time, several laboratories investigated this phenomenon in order to describe its occurrence. The reaction of the

majority of manufacturers was to establish test rigs in order to investigate the specific burner’s weaknesses. Despite the good results provided by this solution, it does not give a full and general understanding of the problem, something indispensable during the design phase. One of the most credited approaches is to investigate the physics behind humming by acoustic simulations so as to foresee typical humming frequencies to be avoided in any given combustion chamber. Though this method provided good results, further investigations pointed out the importance of the mean flow, which was initially neglected, and of other effects which were in early investigations presumed to be negligible. This thesis aims to deepen the importance of mean flow and resulting drawbacks while applying an analytical model that describes combustion instabilities including nonlinear effects.

1.1 Physical explanation

By definition a system is called stable against a perturbation, when its initial conditions are re-established after being perturbed; otherwise it is called unstable. Hence, system stability is often studied by subjecting systems to an initial perturbation and observing reactions. Credit for having first observed combustion oscillations goes to Byron Higgins, in 1777 [1], but it was only in 1878 that Lord Rayleigh theorized the onset of instabilities and started developing a theory based on phenomenological observation [3]. Rayleigh’s theory has been refined over time by various scientists and can now be expressed in the following form:

$$\int_0^{t_{period}} \int_0^V p'(x, t) q'(x, t) dv dt > 0, \quad (1.1)$$

where p' and q' represent pressure and heat release fluctuations. Integrals are calculated over oscillation period and control volume. Assuming pressure and heat release fluctuations to be periodic over time, instability occurs when inequality (1.1) is satisfied. For instance, (1.1) is satisfied when p' and q' are in phase. It must be noted that the latter condition is necessary but not sufficient. The reason lies in the right hand side of inequality (1.1): interaction between pressure and heat release must also overcome losses for an instability to initiate. It can be very helpful to see the problem from a thermodynamic point of view. The following simple yet effective way to understand instability has been provided by W. Polifke [4]. Sound waves are isentropic and therefore the volume moves along an isentropic line on the plane (v, p) , where p is pressure and v the specific volume. When heat is added to or extracted from the gas, an increase or decrease - of specific volume occurs. If heat addition is periodic and in phase with pressure oscillations, the gas volume moves clockwise around the plane (v, p) , forming a thermodynamic cycle. This cycle develops a self-excited instability when energy input transferred from the flame to the acoustic flame is higher than losses. Else, if the two fluctuations are not perfectly in phase, the thermodynamic cycle will be smaller

and less efficient. Lastly, if the two are completely out-of-phase, the gas volume moves counterclockwise, developing a thermodynamic cycle that extracts mechanical energy from the acoustic wave.

1.2 Academic approach

Despite the aforementioned integral form, Rayleigh criterion is still difficult to apply because no explicit information about frequency spectrum or flame shape is available. Hence, fulfillment of equation (1.1) should be verified for every possible frequency spectrum and any flame shape admitted by the equations of motion. This control is practically impossible so that, at the moment, Rayleigh criterion is correct but useless. This is the reason why different authors provided different methods to take into account thermoacoustic interactions. Indeed, there are several mechanisms leading to instability, and, correspondingly, many competing theories are available. Except for the literature cases described in Chapter 2, this thesis is based on a proprietary model of Ansaldo Energia. Due to the importance given to injection conditions, this model shows some similarities to work done by Lieuwen and Cho [5]. To date, most models neglect both mean flow and entropy waves (see Appendix I). This simplification, as pointed out by Dowling [6], is not negligible and may modify consistently resonant frequencies, as seen by Nicoud and Wieczorek [7]. The problem is that entropy waves, or convected hot spots, become coupled with acoustic waves and their strength is highly affected by spatial distribution of heat input. Considering the flame as a plane of negligible thickness is another common simplification, so it's easy to understand the reason of those arrangements. Therefore, results obtained when not considering those two effects may be misleading and must be handled with care. A central feature of most theories is the so-called Flame Transfer Function, or FTF, which represents the mechanism that couples pressure perturbation with heat release. FTF may be seen as a transducer with gain as in Fig. 1.1.



Figure 1.1: FTF

But a similar interpretation would be misleading both when estimating the FTF from measurements and when using it in a numerical model: a feedback must be included as in Fig. 1.2.

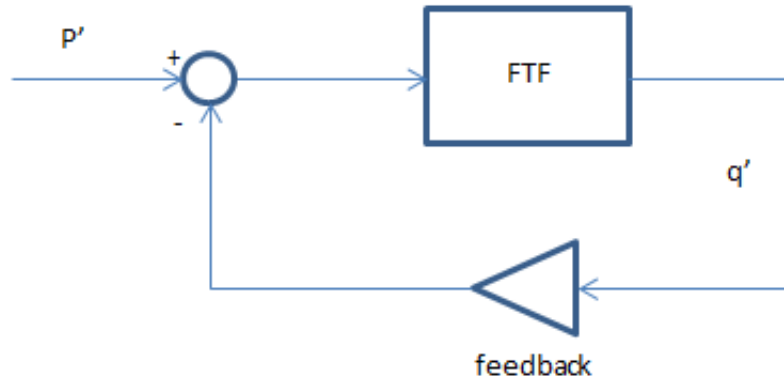


Figure 1.2: FTF with feedback

In spite of its simplicity, this scheme is crucial for the correct representation of a system that may self-induce instability. In fact the first cycle, being open, may only amplify or damp an oscillation; while the second scheme, being closed, may start oscillating by itself.

1.3 Ansaldo Energia's approach

To date, Ansaldo Energia aims at predicting combustion instabilities with the help of the following approaches:

- measurements on single burners in atmospheric pressure and full annular burners in operating pressure;
- finite-volume based commercial software (ANSYS Fluent) to perform thermal fluid dynamics analysis on burners and combustion chambers (both in-house and third part commissioned studies);
- lumped parameters tool (LOMTI) in collaboration with DICAT (Universit di Genova) to study, in the frequency domain, combustors modeled as acoustic networks [8];
- finite-element based commercial software (COMSOL Multiphysics) to perform acoustic and thermo-acoustic frequency studies in partnership with Politecnico di Bari [9];
- models of interaction between pressure oscillations and flame (FTF)

Typically, finite-volume software and finite-element software are used together: results obtained with one software are used as input into the other to find the Flame Transfer Function, basically echoing the feedback scheme of Fig. 1.2. This approach is probably the best way to shape the FTF, but the enormous computational effort of a precise finite-volume analysis significantly limits the number of interactions between the two codes. Unfortunately, LOMTI suffers of important geometry simplification that made it unsuitable when studying real combustion chambers, so it was abandoned in favor of commercial software. Given the good results obtained by using COMSOL Multiphysics (from now on: CM), this software was adopted by AE to continue the investigation of this problem.

Chapter 2

Effects of the mean flow: a literature case

Before introducing AE's model describing heat release, the effects of a mean flow are studied. The availability of a reliable evaluation of the velocity field from previous finite-volume studies and being able to consider the real geometry with CM, render it apparently straightforward to evaluate how frequencies found from thermoacoustic studies are shifted when a mean flow is included. Hence, in this section, a literature case showing the importance of Mach number is replicated using the "Acoustic module" of CM. As said, when studying thermoacoustic instabilities, the assumption of zero mean flow has been a standard for long. Taking into account the results achieved by Dowling and Stow [10] and Nicoud & Wieczorek [7] an academic configuration has been modeled using CM in order to replicate one of Nicoud's and Wieczorek's experiments, which underlined a strong dependency between the Mach number and the model's eigenfrequencies when unsteady heat release is considered. The aim of this experiment is to observe the eventual shift in frequency when considering the mean flow. Indeed, the original intention of this experiment was to compare the results obtained from two different methods used to solve the eigenvalue problem. However, this configuration has proved to be an interesting case and has therefore been chosen as a benchmark from the literature. To study the dependence from the mean flow, a parametric sweep on the inlet Mach number has been set up.

2.1 Equations of thermo-acoustic

The wave equation, used for the resolution of the acoustic analysis, is derived from the linearized equations of conservation. Being the fluid compressible, viscous and neglecting the effect of any external force, the equations that represent conservation of mass, momentum and energy are:

$$\frac{D\rho}{Dt} + \rho \nabla \cdot \mathbf{u} = 0, \quad (2.1)$$

$$\rho \frac{D\mathbf{u}}{Dt} = -\nabla p + \frac{\partial \sigma_{i,j}}{\partial x_j} \mathbf{e}_i, \quad (2.2)$$

$$\rho \frac{Dh}{Dt} = \frac{Dp}{Dt} + q + \nabla \cdot (K \nabla T) + \sigma_{i,j} \frac{\partial u_i}{\partial x_j}. \quad (2.3)$$

Where \mathbf{u} is the velocity vector, $\sigma_{i,j}$ is the viscous stress tensor, K is the thermal conductivity and q is the heat rate added per unit volume. Assuming the gas as perfect, equation (2.4) is introduced. This implies that specific heats are constant:

$$\frac{p}{\rho} = RT. \quad (2.4)$$

Combining equations (2.2), (2.3), (2.4) and defining entropy by (2.5), (2.6) and (2.7) yields equation (2.8)

$$dh = T dS + \frac{1}{\rho} dp, \quad (2.5)$$

$$S = c_v \log\left(\frac{p}{\rho^\gamma}\right), \quad (2.6)$$

$$\gamma = \frac{c_p}{c_v}, \quad (2.7)$$

$$\rho T \frac{DS}{Dt} = q + \nabla \cdot (K \nabla T) + \sigma_{i,j} \frac{\partial u_i}{\partial x_j}. \quad (2.8)$$

Now, considering each variable as a composition of a steady uniform part and a small perturbation, such as

$$p(\mathbf{x}, t) = \bar{p} + p'(\mathbf{x}, t), \quad (2.9)$$

the linearized equations for the perturbations, neglecting viscous stresses and thermal conductivity, are obtained:

$$\frac{\bar{D}\rho'}{Dt} + \bar{\rho} \nabla \cdot \mathbf{u}' = 0, \quad (2.10)$$

$$\rho \frac{\bar{D}\mathbf{u}'}{Dt} + \frac{1}{\bar{\rho}} \nabla \cdot p' = 0, \quad (2.11)$$

$$\bar{\rho} \bar{T} \frac{\bar{D}S'}{Dt} = q'. \quad (2.12)$$

Combining the previous three equations under the hypothesis that $S' = \frac{c_v p'}{\bar{p}} - \frac{c_p p'}{\bar{\rho}}$, the inhomogeneous wave equation is obtained:

$$\frac{1}{\bar{c}^2} \frac{\bar{D}^2 p'}{Dt^2} - \nabla^2 p' = \frac{\gamma - 1}{\bar{c}^2} \frac{\partial q'}{\partial t}. \quad (2.13)$$

When the flow velocity is acceptably lower than the sound velocity, \bar{u} can be considered negligible. Thus, being $\frac{\bar{D}}{Dt} = \frac{\partial}{\partial t} + \bar{\mathbf{u}} \cdot \nabla$ as in [10], equation (2.13) becomes:

$$\frac{1}{\bar{c}^2} \frac{\partial^2 p'}{\partial t^2} - \nabla^2 p' = \frac{\gamma - 1}{\bar{c}^2} \frac{\partial q'}{\partial t}. \quad (2.14)$$

2.2 Introducing unsteady heat release and mean flow into CM's "Pressure Acoustics" module

In order to study this configuration, the "Pressure Acoustics" module available in CM has been used. The "Pressure Acoustics" module is based on the following inhomogeneous Helmholtz equation, written in the frequency domain:

$$\nabla \cdot \left[-\frac{1}{\rho_c} (\nabla p - \mathbf{q}) \right] - \frac{\omega^2 p}{\rho_c c^2} = \mathbf{Q}, \quad (2.15)$$

where:

$$k_{eq}^2 = \left(\frac{\omega}{c} \right)^2, \quad (2.16)$$

$$\lambda = -i\omega. \quad (2.17)$$

In order to consider into equation (2.15) the terms due to unsteady heat release and mean flow, the inhomogeneous wave equation written in the frequency domain is taken into account:

$$\begin{aligned} \lambda^2 \hat{p} - c^2 \nabla^2 \hat{p} = & (\gamma - 1) \left(-\lambda \hat{q} + \bar{u}_x \frac{\partial \hat{q}}{\partial x} + \bar{u}_y \frac{\partial \hat{q}}{\partial y} + \bar{u}_z \frac{\partial \hat{q}}{\partial z} \right) \\ & + 2\lambda \bar{u}_x \frac{\partial \hat{p}}{\partial x} + 2\lambda \bar{u}_y \frac{\partial \hat{p}}{\partial y} + 2\lambda \bar{u}_z \frac{\partial \hat{p}}{\partial z} - \bar{u}_x^2 \frac{\partial^2 \hat{p}}{\partial x^2} - \bar{u}_y^2 \frac{\partial^2 \hat{p}}{\partial y^2} - \bar{u}_z^2 \frac{\partial^2 \hat{p}}{\partial z^2} \\ & - \bar{u}_x \bar{u}_y \frac{\partial^2 \hat{p}}{\partial x \partial y} - \bar{u}_x \bar{u}_z \frac{\partial^2 \hat{p}}{\partial x \partial z} - \bar{u}_y \bar{u}_z \frac{\partial^2 \hat{p}}{\partial y \partial z} - \bar{u}_x \frac{\partial \bar{u}_x}{\partial x} \frac{\partial \hat{p}}{\partial x} - \bar{u}_y \frac{\partial \bar{u}_y}{\partial y} \frac{\partial \hat{p}}{\partial y} - \bar{u}_z \frac{\partial \bar{u}_z}{\partial z} \frac{\partial \hat{p}}{\partial z} \\ & - \bar{u}_x \frac{\partial \bar{u}_y}{\partial x} \frac{\partial \hat{p}}{\partial y} - \bar{u}_x \frac{\partial \bar{u}_z}{\partial x} \frac{\partial \hat{p}}{\partial z} - \bar{u}_y \frac{\partial \bar{u}_x}{\partial y} \frac{\partial \hat{p}}{\partial x} - \bar{u}_y \frac{\partial \bar{u}_z}{\partial y} \frac{\partial \hat{p}}{\partial z} - \bar{u}_z \frac{\partial \bar{u}_x}{\partial z} \frac{\partial \hat{p}}{\partial x} - \bar{u}_z \frac{\partial \bar{u}_y}{\partial z} \frac{\partial \hat{p}}{\partial y}. \end{aligned} \quad (2.18)$$

The switch to the frequency domain has been made possible by the assumption that space and time dependencies can be split.

$$p'(x, t) = \Re [\hat{p}(x)e^{i\omega t}]; \quad q'(x, t) = \Re [\hat{q}(x)e^{i\omega t}]. \quad (2.19)$$

After some manipulations, the terms on the right side of equation (2.18), representing the mean flow and the unsteady heat release, are then inserted into (2.15) inside terms \mathbf{Q} and \mathbf{q} . This allows us to include the effects of the mean flow inside the whole domain despite the simplifications under which equation (2.14) was written. As for the heat release, Nicoud and Wiczorek provide the following expression:

$$\hat{q}(\mathbf{x}) = \frac{q_{tot}}{U_{bulk}} n_u(\mathbf{x}) e^{i\omega\tau_u(x)} \hat{\mathbf{u}}(\mathbf{x}_{ref}) \cdot \mathbf{n}_{ref}, \quad (2.20)$$

where:

$$\begin{cases} n_u(x) = \frac{n^*}{\delta_f} \cdot \frac{\bar{u}_{in}}{q_{tot}} \cdot \frac{\gamma p_0}{\gamma - 1}, & \text{if } x_f - \frac{\delta_f}{2} < x < x_f + \frac{\delta_f}{2}, \\ n_u(x) = 0, & \text{elsewhere.} \end{cases} \quad (2.21)$$

Note that \mathbf{n}_{ref} is a unitary vector defining the direction of the reference velocity and U_{bulk} has been used in 2.20 to make sure that the heat release locator $n_u(x)$ is dimensionless.

2.3 Geometry and data

Geometry, originally one-dimensional, has been modeled as three-dimensional for a better visualization, under consideration that the lack of viscous terms into the pressure acoustic module makes the problem independent from the radius. Geometry is shown in Fig. 2.1. The nozzle has been modeled to satisfy both continuity equation and Mach number. This is also how the radius was estimated.

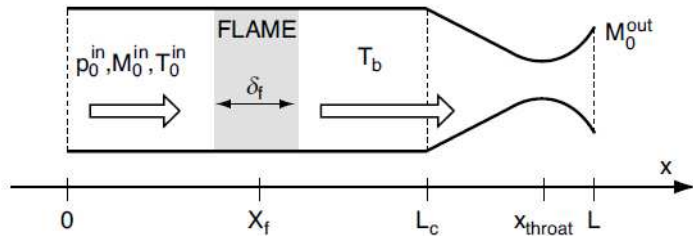


Figure 2.1: Original duct configuration

The resulting geometry consists of a mesh of 4603 elements (2433 tetrahedral), provided by CM's embedded mesher. A fine mesh is required in order to ensure the necessary number of elements needed to resolve each wavelength, also considering that both \mathbf{Q} and \mathbf{q} contain a first order derivative of \hat{p} .

Geometrical and physical data are listed in Tab. 2.1.

Table 2.1: various data

| Name | Value | Description |
|----------------|------------|---|
| L | 1.1 m | Length of the duct |
| L_c | 1 m | Length of the duct except the nozzle |
| rad | 0.02 m | Radius of the duct |
| δ_f | 0.15 m | Flame thickness |
| x_f | 0.5 m | Flame position |
| X_{throat} | 1.0863 m | Throat position |
| p_0 | 101 325 Pa | Initial pressure |
| $T_{0,inlet}$ | 300 K | Temperature before the flame |
| $T_{0,outlet}$ | 1200 K | Temperature after the flame |
| T_0 | Eq. (2.22) | Temperature profile through the duct |
| Ma_{inlet} | 0.05 | Mach number in the duct when considering non-zero Mach flow |
| Ma_{outlet} | 1.5 | Mach number in the nozzle |
| τ | 0.001 s | Residence time |
| n^* | 5 | Order of reaction |

The temperature inside the flame zone is given

$$T_0 = \frac{T_{0,inlet} + T_{0,outlet}}{2} + \frac{T_{0,outlet} - T_{0,inlet}}{2} \tanh\left(3\frac{x - x_f}{\delta_f}\right). \quad (2.22)$$

The boundary condition at the inlet is the following: $\hat{u} = 0$. To simulate it in CM, the *Sound Hard Boundary* shown in equation (2.24) has been used. This condition is, in fact, a manipulation of equation (2.23), where Z_i is the acoustic impedance:

$$-n \cdot \left[-\frac{1}{\rho_c} (\nabla p_i - q) \right] = -p_t \frac{i\omega}{Z_i}, \quad (2.23)$$

$$-n \cdot \left[-\frac{1}{\rho_c} (\nabla p_i - q) \right] = 0. \quad (2.24)$$

It must be noted that, for the software employed, to impose a sound hard boundary is equivalent to consider null the pressure gradient. Considering momentum continuity described in the linearized Euler equation (2.2), this is equal to consider a vanishing material derivative of velocity. However, being the mean flux left out from the Pressure Acoustics module, material derivative is equal to the time derivative. This means that, when trying to express the boundary condition $\hat{u} = 0$, the software indeed expresses $\frac{\partial \hat{u}}{\partial t} = 0$. This generates errors especially in the consideration of the imaginary part of the eigenfrequencies, and it's an approximation due to the chosen module. At the outlet, being the nozzle choked, it is not necessary to specify a boundary condition. This also means that, for the acoustic solver, the only part of the duct that plays a role in the computation of the eigenfrequencies is the one upstream of the nozzle throat. However, a sound hard boundary is also imposed at the end of the duct.

2.4 Results and observations

Obtained and expected frequencies for the first mode are listed in Tab. 2.2.

Table 2.2: obtained and expected frequencies

| Ma_{inlet} | Obtained frequency | Expected frequency |
|---------------------|--------------------|--------------------|
| 0 | $186.35 - 2.6i$ | $183 - 2i$ |
| 0.05 | $232.36 + 12i$ | $234 + 32i$ |

What first stands out is the good accuracy of the real part of the frequencies compared to the imaginary part. These differences are in fact more important than it seems, as we know by theory that the system should have imaginary part equal to zero or at least slightly positive, given that the only stability modifier is the heat release. It must be said that even Nicoud and Wieczorek pointed out some numerical differences depending on the method used to solve the eigenfrequency problem, so it is reasonable to assume that a part of the inconsistencies found may be due to the use of a different solver. Fig. 2.2 and Fig. 2.3 show further agreement between expected and obtained results.

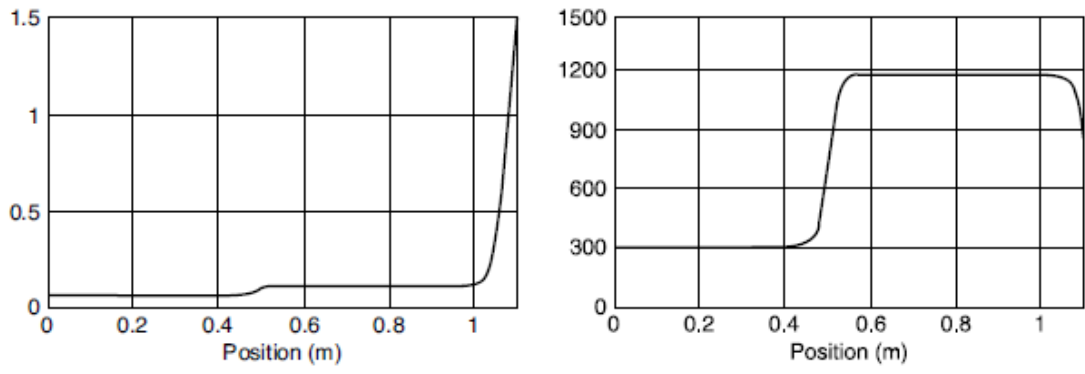


Figure 2.2: Mach (left) and temperature (right) profiles from Nicoud and Wieczorek

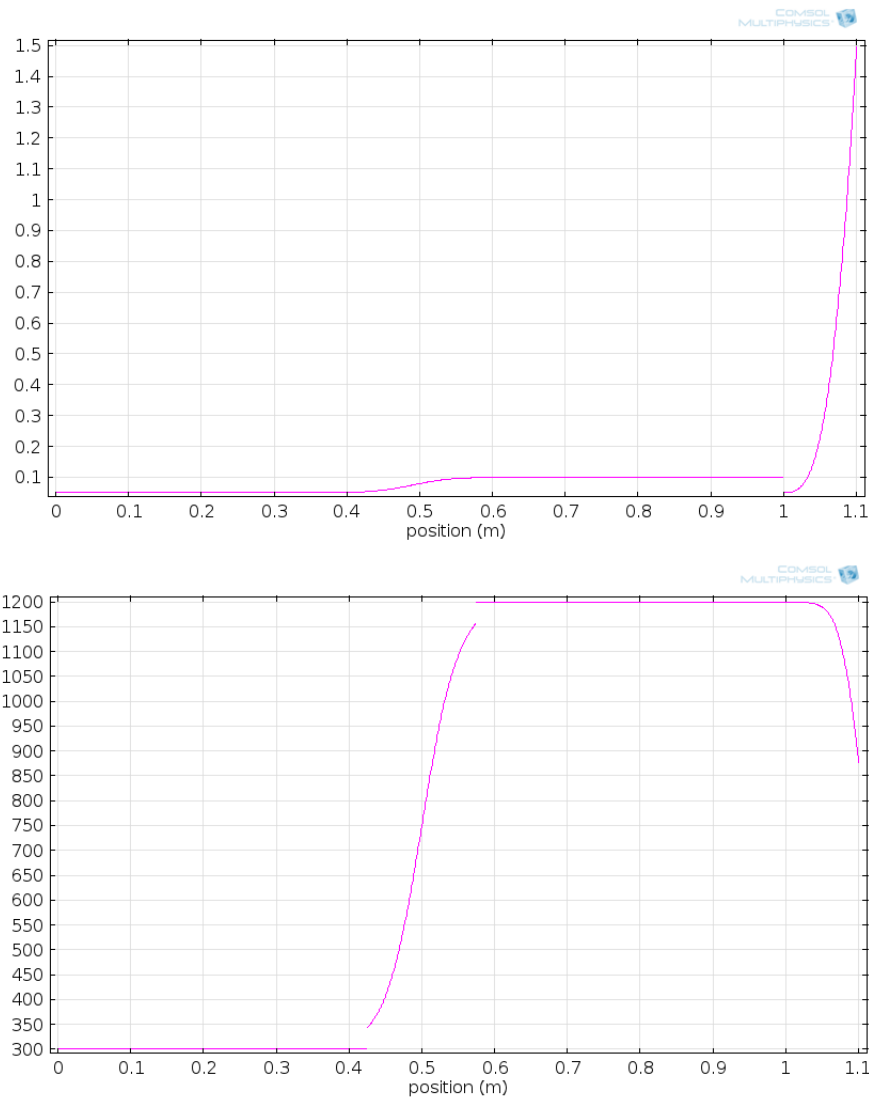


Figure 2.3: Mach (above) and temperature (below) profiles imposed using COMSOL Mutiphysics

Discontinuities in the temperature profile in Fig. 2.3 are caused by equation (2.22) itself. These discontinuities could in fact introduce some convergence problems. Therefore, developing a new equation to describe a temperature profile that connects smoothly T_{inlet} and T_{outlet} should be taken into account. Overall, the literature case has been well represented and seems to validate the use of the Acoustic module when considering the mean flow.

Chapter 3

Importance of a uniform mean flow

It must be noted that the case depicted in the previous chapter does not consider viscosity but, given the duct's shape, implicitly states that mean flow is not uniform. This assumption is much more relevant than it could appear, as it is the only one that allows us to study our problem in frequency. In fact we used an eigenfrequency solver while tacitly expecting humming frequencies to be well separated from each other. Indeed, such expectation agrees with experiments. However, it turns out to be a suitable criterion for solver selection only if the operator acting on the pressure perturbation in the sound equation is Hermitian. The existence of a discrete spectrum of eigenfrequencies is warranted, in fact, for Hermitian operators only with Dirichlet-Neumann boundary conditions. Non-uniform unperturbed flows render the operator above introduced not Hermitian, as we are going to show in the following Section.

3.1 Demonstration that the wave equation with non-uniform mean flow is non-Hermitian

An Hermitian¹ (or self-adjoint) operator L acting on the integrable functions defined on the real interval $D \in \Re$ satisfies the identity $\int_D dx f^*(Lg) = \int_D dx (Lf^*)g$ for an arbitrary couple of functions f and g , where f^* is the complex conjugate of f . Expansion to multidimensional $D \in \Re^n$ is straightforward. Given equations (3.1), we verify if the operator $\left(\frac{D}{Dt^2} - c^2\nabla^2\right)$ is Hermitian.

$$\left\{ \begin{array}{l} \frac{D^2 p'}{Dt^2} - c^2 \nabla^2 p' = 0 \\ \frac{\partial \bar{u}}{\partial t} = 0 \end{array} \right. \quad (3.1)$$

¹See equations 14.4.4, 15.2.1 and following, and 14.8-4 of Korn, G. A. & Korn, Th. M., Mathematical Handbook For Scientists And Engineers, McGraw-Hill, New York, 1968.

$$\begin{aligned}
L &= \left(\frac{\partial}{\partial t} + \bar{u} \frac{\partial}{\partial x} \right)^2 = \left(\frac{\partial}{\partial t} + \bar{u} \frac{\partial}{\partial x} \right) \left(\frac{\partial}{\partial t} + \bar{u} \frac{\partial}{\partial x} \right) = \\
&= \underbrace{\frac{\partial^2}{\partial t^2}}_{A_1} + \underbrace{\bar{u} \frac{\partial}{\partial x} \left(\bar{u} \frac{\partial}{\partial x} \right)}_{A_2} + \underbrace{2\bar{u} \frac{\partial}{\partial t} \frac{\partial}{\partial x}}_{A_3}
\end{aligned} \tag{3.2}$$

$$\iint f L g dx dt = \iint f A_1 g dx dt + \iint f A_2 g dx dt + \iint f A_3 g dx dt \tag{3.3}$$

$$\begin{aligned}
\iint f A_1 g dx dt &= \iint f \frac{\partial^2}{\partial t^2} g dx dt = \int dx \int \frac{\partial}{\partial t} \left(f \frac{\partial g}{\partial t} \right) dt \\
&- \int dx \int \frac{\partial f}{\partial t} \frac{\partial g}{\partial t} dt = \int dx \int \frac{\partial}{\partial t} \left(f \frac{\partial g}{\partial t} \right) dt - \iint \frac{\partial}{\partial t} \left(g \frac{\partial f}{\partial t} \right) dx \\
&+ \iint dx g \frac{\partial^2 f}{\partial t^2} dt = \iint dx \underbrace{\frac{\partial^2}{\partial t^2} \left(f \frac{\partial g}{\partial t} - g \frac{\partial f}{\partial t} \right)}_{B_1} dt + \iint dx g \frac{\partial^2 f}{\partial t^2} dt
\end{aligned} \tag{3.4}$$

If $B_1 = 0$ (Dirichlet² or Neumann³ boundary conditions):

$$\int dx \int f \frac{\partial^2}{\partial t^2} g dt = \int dx \int g \frac{\partial^2}{\partial t^2} f dt \tag{3.5}$$

Then A_1 is Hermitian.

$$\begin{aligned}
\int dx f A_2 g &= \int dx f \bar{u} \frac{\partial}{\partial x} \left(\bar{u} \frac{\partial g}{\partial x} \right) = \int dx \left(f \bar{u}^2 \frac{\partial^2 g}{\partial x^2} + f \bar{u} \frac{\partial \bar{u}}{\partial x} \frac{\partial g}{\partial x} \right) = \\
&\int dx \frac{\partial}{\partial x} \left(f \bar{u}^2 \frac{\partial g}{\partial x} \right) - \int dx \frac{\partial}{\partial x} (f \bar{u}^2) \frac{\partial g}{\partial x} + \int dx f \frac{\partial g}{\partial x} \left(\frac{\partial \bar{u}^2}{\partial x} \right) = \\
&\int dx \frac{\partial}{\partial x} \left(f \bar{u}^2 \frac{\partial g}{\partial x} \right) - \int dx \frac{\partial}{\partial x} \left[\frac{\partial}{\partial x} (f \bar{u}^2) g \right] + \int dx g \frac{\partial^2}{\partial x^2} (f \bar{u}^2) + \\
&+ \int dx f \frac{\partial g}{\partial x} \left(\frac{\partial \bar{u}^2}{\partial x} \right) = \underbrace{\int dx \frac{\partial}{\partial x} \left[\frac{\partial g}{\partial x} - g \frac{\partial}{\partial x} (f \bar{u}^2) \right]}_{C_1} + \int dx g \frac{\partial^2}{\partial x^2} (f \bar{u}^2) + \\
&+ \underbrace{\int dx \frac{\partial}{\partial x} \left(f g \frac{\partial \bar{u}^2}{\partial x} \right) - \int dx g \frac{\partial}{\partial x} \left[f \left(\frac{\partial \bar{u}^2}{\partial x} \right) \right]}_{C_2}
\end{aligned} \tag{3.6}$$

²Value of function at the boundary is imposed.

³Value of function's derivative at the boundary is imposed.

If $C_1 = 0$ and $C_2 = 0$ (Dirichlet or Neumann boundary conditions):

$$\left\{ \begin{array}{l} \frac{\partial}{\partial x} (f\bar{u}^2) = \bar{u}^2 \frac{\partial f}{\partial x} + f \frac{\partial \bar{u}^2}{\partial x} = \bar{u}^2 \frac{\partial f}{\partial x} + 2\bar{u}^2 f \frac{\partial \bar{u}}{\partial x} \\ \frac{\partial^2}{\partial x^2} (f\bar{u}^2) = \bar{u}^2 \frac{\partial^2 f}{\partial x^2} + 4\bar{u}^2 \frac{\partial f}{\partial x} \frac{\partial \bar{u}}{\partial x} + 2f \left(\frac{\partial \bar{u}}{\partial x} \right)^2 + 2\bar{u} f \frac{\partial^2 \bar{u}}{\partial x^2} \\ \frac{\partial}{\partial x} \left(\frac{\partial \bar{u}^2}{\partial x} f \right) = \frac{\partial f}{\partial x} \left(\frac{\partial \bar{u}^2}{\partial x} f \right) + f \frac{\partial}{\partial x} \left(\frac{\partial \bar{u}^2}{\partial x} f \right) \end{array} \right. \quad (3.7)$$

$$\begin{aligned} \iint dt dx f A_2 g &= \iint dt dx f \bar{u} \frac{\partial}{\partial x} \left(\bar{u} \frac{\partial g}{\partial x} \right) = C_1 + \underbrace{\int dt \int dx g \bar{u}^2 \frac{\partial^2 f}{\partial x^2}}_{\iint dt dx g \bar{u}^2 A_2 f} + \\ &+ 4 \iint dt dx \bar{u} g \frac{\partial f}{\partial x} \frac{\partial \bar{u}}{\partial x} + 2 \iint dt dx g f \left(\frac{\partial \bar{u}}{\partial x} \right)^2 + 2 \iint dt dx g \bar{u} f \frac{\partial^2 \bar{u}}{\partial x^2} + \\ &+ C_2 - \iint dt dx g \frac{\partial f}{\partial x} \left(\frac{\partial \bar{u}^2}{\partial x} f \right) - \iint dt dx g f \frac{\partial}{\partial x} \left(\frac{\partial \bar{u}^2}{\partial x} \right) \end{aligned} \quad (3.8)$$

$$\begin{aligned} \int dt \int dx f A_3 g &= \int dt \int dx f 2\bar{u} \frac{\partial}{\partial t} \left(\frac{\partial g}{\partial x} \right) = \\ &2 \underbrace{\int dx \bar{u} \int dt \frac{\partial}{\partial t} \left(f \frac{\partial g}{\partial x} \right)}_{D_1} - 2 \int dx \bar{u} \int dt \frac{\partial f}{\partial t} \frac{\partial g}{\partial x} \end{aligned} \quad (3.9)$$

If $D_1 = 0$ (Dirichlet or Neumann boundary conditions):

$$-2 \int dx \bar{u} \int dt \frac{\partial f}{\partial t} \frac{\partial g}{\partial x} = -2 \underbrace{\int dt \int dx \frac{\partial}{\partial x} \left(\bar{u} \frac{\partial f}{\partial t} \frac{\partial g}{\partial x} \right)}_{E_1} + 2 \int dt \int dx g \frac{\partial}{\partial x} \left(\bar{u} \frac{\partial f}{\partial t} \right) \quad (3.10)$$

If $E_1 = 0$ (Dirichlet or Neumann boundary conditions):

$$2 \int dt \int dx g \frac{\partial}{\partial x} \left(\bar{u} \frac{\partial f}{\partial t} \right) = \underbrace{\int dt \int dx g 2\bar{u} \frac{\partial}{\partial t} \left(\frac{\partial f}{\partial x} \right)}_{\iint dx dt g A_3 f} + 2 \int dt \int dx g \frac{\partial f}{\partial t} \frac{\partial \bar{u}}{\partial x} \quad (3.11)$$

Thus, by combining equations (3.5), (3.8) and (3.11), equation (3.3) can be rewritten as:

$$\begin{aligned}
\iint f L g dx dt &= \iint g A_1 f dx dt + \underbrace{\iint g A_2 f dx dt}_{\iint g L f dx dt} \iint g A_3 f dx dt + \\
&+ \iint dx dt \left[4g\bar{u} \frac{\partial \bar{u}}{\partial x} \frac{\partial f}{\partial x} + 2gf \left(\frac{\partial \bar{u}}{\partial x} \right)^2 + 2gf\bar{u} \frac{\partial^2 \bar{u}}{\partial x^2} + 2g \frac{\partial f}{\partial t} \frac{\partial \bar{u}}{\partial x} \right] + \\
&+ \iint dx dt \left[-g \frac{\partial f}{\partial x} \left(\frac{\partial \bar{u}^2}{\partial x} \right) - gf \frac{\partial}{\partial x} \left(\frac{\partial \bar{u}^2}{\partial x} \right) \right]
\end{aligned} \tag{3.12}$$

Therefore L is Hermitian if there are Dirichlet or Neumann boundary conditions to nullify $B_1 C_1 D_1 E_1$ and if $\frac{\partial \bar{u}}{\partial x} = 0$, i.e. the mean flow is uniform in the streamwise direction.

3.2 Impact on our investigation

Our conclusions induce us to prefer the investigation of the instability onset in the time domain rather than in the frequency domain. The reason is briefly explained as follows. Stability analysis is commonly performed by analyzing the imaginary part of the system's eigenfrequencies. Accordingly, to check that the imaginary parts of all eigenfrequencies are negative is enough, for most linear investigations, to claim that the system is stable against all conceivable perturbation. However, this claim is correct only if the eigenvectors of the relevant operator form an orthonormal basis. Intuitively, we may grasp the reason with the help of elementary geometry. Let us draw a segment as the composition of two vectors.

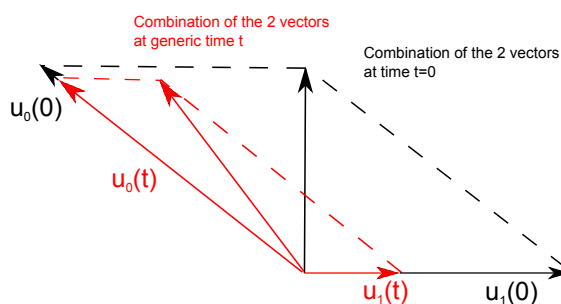


Figure 3.1: Not perpendicular eigenvectors

Moreover, let the length of both vectors decrease monotonically with time, while the angle between the vectors remains constant. Even so, the segment's length is not

bound to decrease monotonically with time, unless the vectors are perpendicular to each other. If this is not the case, the segment's length is allowed to increase transiently, even considerably, before exponential decay. This transient amplification is enough to drive the system outside the domain of validity of a linear treatment in most cases, even if stability analysis would predict stability. In turn, we are sure that the eigenvectors of the relevant operator form an orthonormal basis only if the operator is Hermitian. But we have shown that our operator is generally not Hermitian. Consequently, any stability analysis based on the evaluation of the signs of the imaginary parts of all eigenfrequencies is not completely trustworthy when considering our problem. Of course, this change from the single frequency analysis to the time domain implies a bigger computational effort but guarantees the possibility of representing the much more realistic case of a non-uniform mean flow. An interesting result is that the "benchmark" provided by literature studied in the previous section is not completely erroneous. In fact, obtained results are correct: unfortunately they are meaningful only when the mean flow is uniform. Given the duct's shape, this is definitely out of the question.

Chapter 4

Thermoacoustics with mean flow

Given our previous results, we started developing our own set of equation within CM to perform thermoacoustic studies considering the mean flow. Our approach is mainly inspired by work done by Pankiewicz and Sattelmeyer [11]. Partial differential equations (PDE) here listed are written in weak form using CM's embedded Physic Builder. To give a general understanding of this approach, let us say that the weak formulation generally permits to identify a function through its behavior with respect to a known test function rather than by knowing its value at any given point. For further information about the weak form, the reader is invited to consult [12]. The starting points of our thermoacoustic study are the same conservation equations used for a viscous compressible Newtonian fluid formerly used to find the inhomogeneous wave equation: mass (4.1), momentum (4.2) and energy (4.3) conservation.

$$\frac{D\rho}{Dt} + \rho \nabla \cdot \mathbf{u} = \frac{\partial \rho}{\partial t} + \rho \nabla \cdot \mathbf{u} = 0, \quad (4.1)$$

$$\rho \frac{D\mathbf{u}}{Dt} = \nabla \cdot \left[-p\mathbf{I} + \mu_0 (\nabla \mathbf{u} + \nabla \mathbf{u}^T) + \frac{2}{3}\mu_B (\nabla \cdot \mathbf{u}) \mathbf{I} \right], \quad (4.2)$$

$$\begin{aligned} \rho T \frac{DS}{Dt} &= \rho T \left[\left(\frac{\partial S}{\partial T} \right)_p \frac{DT}{Dt} + \left(\frac{\partial S}{\partial p} \right)_T \frac{Dp}{Dt} \right] = \\ &= q + \nabla \cdot (K \nabla T) \rightarrow \rho c_p \frac{DT}{Dt} - \alpha T \frac{Dp}{Dt} = q + \nabla \cdot (K \nabla T) + \phi, \end{aligned} \quad (4.3)$$

since $\left(\frac{\partial S}{\partial p} \right)_T = - \left(\frac{\partial V}{\partial p} \right)_p = - \left[\frac{\partial}{\partial T} \left(\frac{1}{\rho} \right) \right]_p = \frac{1}{\rho^2} \left(\frac{\partial \rho}{\partial T} \right) = \frac{\alpha}{\rho}$ and $\left(\frac{\partial S}{\partial T} \right)_p = \frac{c_p}{T}$.

As for equation (4.2), the fluid is assumed to be isotropic, as valid for gases and simple liquids.

4.1 Linearization of equations

For small oscillations, equation (2.9) is valid. Both dependent variables and sources may be considered in the form of a mean value plus a first order perturbation. Conservation equations become:

$$\frac{\partial \rho'}{\partial t} + \nabla \cdot \rho' \bar{\mathbf{u}} + \nabla \cdot \bar{\rho} \mathbf{u}' = 0, \quad (4.4)$$

$$\begin{aligned} & \bar{\rho} \left[\frac{\partial \mathbf{u}'}{\partial t} + \bar{\mathbf{u}} \cdot \nabla \mathbf{u}' + \mathbf{u}' \cdot \nabla \bar{\mathbf{u}} \right] + \rho' \bar{\mathbf{u}} \cdot \nabla \bar{\mathbf{u}} = \\ & = \nabla \cdot \left[-p' \mathbf{I} + \mu_0 \left(\nabla \mathbf{u}' + \nabla \mathbf{u}'^T \right) + \frac{2}{3} \mu_B \nabla \cdot \mathbf{u}' \mathbf{I} \right], \end{aligned} \quad (4.5)$$

$$\begin{aligned} & \rho' c_p \bar{\mathbf{u}} \cdot \nabla \bar{T} + \rho c_p \left[\frac{\partial T'}{\partial t} + \bar{\mathbf{u}} \cdot \nabla T' + \mathbf{u}' \cdot \nabla \bar{T} \right] - \alpha_0 T' \bar{\mathbf{u}} \cdot \nabla \bar{p} + \\ & - \alpha_0 \bar{T} \left[\frac{\partial p'}{\partial t} + \bar{\mathbf{u}} \cdot \nabla p' + \mathbf{u}' \cdot \nabla \bar{p} \right] = \nabla \cdot K \nabla T' + q' + \phi_{10}, \end{aligned} \quad (4.6)$$

where ϕ_{10} is the viscous dissipation function defined as follows:

$$\begin{aligned} \phi_{10} = & \nabla \mathbf{u}': \left[\mu_0 \left(\nabla \bar{\mathbf{u}} + \nabla \bar{\mathbf{u}}^T \right) + \left(\mu_B - \frac{2}{3} \mu_0 \right) \nabla \cdot \bar{\mathbf{u}} \mathbf{I} \right] + \\ & + \nabla \bar{\mathbf{u}}: \left[\mu_0 \left(\nabla \mathbf{u}' + \nabla \mathbf{u}'^T \right) + \left(\mu_B - \frac{2}{3} \mu_0 \right) \nabla \cdot \mathbf{u}' \mathbf{I} \right] \end{aligned} \quad (4.7)$$

To close the problem, which has 6 dependent variables ($p', T', u', v', w', \rho'$) for 5 equations, the state equation reported in (4.8) is included.

$$\rho' = p \left(\frac{\partial \rho}{\partial p} \right)_{\bar{p} \bar{T}} + T \left(\frac{\partial \rho}{\partial T} \right)_{\bar{p} \bar{T}} = \bar{\rho} \left(\frac{p'}{\bar{p}} - \frac{T'}{\bar{T}} \right) = \bar{\rho} (p' \beta_T - T' \alpha_0). \quad (4.8)$$

Due to its simplicity, this equation is set in algebraic form rather than in the weak form to limit the matrices size and lighten computation.

4.2 Boundary conditions

Boundary conditions are of fundamental importance when facing our problem. The Rayleigh criterion should in fact take into account, on the right hand side of inequality (1.1), the energy loss through the boundaries. For example, by imposing $\mathbf{u}' = 0$ on

both ends, we are not letting energy go away from the system. In this case, it would not be surprising to see perturbations grow rapidly without reaching stable conditions. The following equations can help us describing how energy remains trapped in:

$$\int_{boundary} \langle p\bar{\mathbf{u}} \rangle \cdot d\Omega. \quad (4.9)$$

Equation (4.9) shows the power lost through a boundary, where angle brackets indicate the following operator:

$$\langle f(t') \rangle = \lim_{T \rightarrow \infty} \left[\frac{\int_t^{T+t} f(t') dt'}{T} \right]. \quad (4.10)$$

Since pressure and velocity are linearized in our system, equation (4.9) can be rewritten as:

$$\int_{boundary} \langle p\bar{\mathbf{u}} \rangle \cdot da = \int \bar{p}\bar{\mathbf{u}} \cdot da + \int \bar{p}\langle \mathbf{u}' \rangle \cdot da + \int da \cdot \bar{\mathbf{u}}\langle p' \rangle + \int \langle p' \mathbf{u}' \rangle \cdot da. \quad (4.11)$$

We now consider the terms on the right hand side. The first term is the loss of mean power never taken into consideration by our model, since it does not correspond to disturbances. The second and third terms vanish because the mean value over time of a perturbation is zero, so the fourth term is the only one left. It is easy to see that when imposing zero perturbation of velocity on the outlet boundary we prevent power from leaving the system. Same goes for ($p' = 0$). This makes us aware of the importance of knowing the modeled system's acoustic impedance at the boundaries, not to mention how difficult it is to gather such information, being the acoustic impedance typically frequency-dependent. Subsequent models will point out consequences of totally reflecting boundaries on different geometries.

4.3 Time step and mesh size

In models studied using our set of equations, we choose minimum element size accordingly to the geometry considered. In most models, the flame thickness is assumed as the minimum element size. Using inequality shown in (4.12), which is basically the Courant-Friedrichs-Lewy condition, the time step is consequently given:

$$\Delta t \cdot c \leq \text{coeff. } d_{mesh}. \quad (4.12)$$

This approach was suggested by CM software support team in order to achieve convergence. Coefficient on the right hand side of the inequality is less than 1: the lower its value the more numerically stable the system is.

Chapter 5

Heat release model

The present, analytical model has been originally developed in Ansaldo Energia in order to investigate limit cycles. Validation was performed by considering realistic numerical values measured in AE's test rig in Sesta, which can be found in Tab. 5.1. For simplicity, the lean combustion of a perfectly premixed mixture of air and fuel only is considered. The Mach number is supposed to be far from one and the total pressure is the same everywhere. Combustion occurs at the flame only, and the mean temperature before and after the flame is given. Fuel inlet pressure is constant. The flame is a thin layer with constant thickness δ_f which separates regions with burnt from unburnt gases. For simplicity, the flame is supposed to be both axisymmetric and free to move, and have also parabolic profile at all times; in simulations run with CM, those assumption may vary or be modeled as concentrated effects. However, the nature and the extent of differences from the analytical model will be further discussed. As stated above, this model's purpose is to study the onset of a limit cycle. Among all mechanisms that may trigger it, only one has been chosen: the simplest. This model therefore leads to a limit cycle in just one variable, the air molar fraction.

$$z = \frac{n_{air}}{n_{air} + n_{fuel}}. \quad (5.1)$$

The present theory assumes that heat source oscillations are started by air molar fraction oscillations convected from the inlet to the flame, following equation (5.2):

$$\frac{Dz}{Dt} = 0. \quad (5.2)$$

At the inlet, air molar fraction depends on pressure perturbations. The feedback mechanism is closed considering that an oscillating heat source produces pressure perturbations that eventually reach the inlet as described by the wave equation (2.14). In order to investigate oscillations of the variable z with given period τ_p , the analytical model introduces the so-called return map:

$$z_{n+1} = z_{n+1}(z_n), \quad (5.3)$$

where $z_n = z(t)$, $z_{n+1} = z(t + \tau_p)$, $z_{n+2} = z(t + 2\tau_p)$ and so on. Steady states correspond to constant z . The oscillating state of period τ_p , representing humming, occurs when $z_{n+1} \neq z_n$ but $z_{n+2} = z_n$ and so on. Therefore, z keeps oscillating between z_n and z_{n+1} , respectively called z_{min} and z_{max} . Investigation of the return map leads to interesting results, though strongly depending on the geometry and on the Mach number. This approach has three main drawbacks:

- it assumes that the flow before the flame is uniform;
- it assumes that the flame is axisymmetric at all times;
- since the return map involves only one physical quantity, only one humming frequency is taken into account

The last one is true for the analytical model in its first form: using only the wave equation it could only have one humming frequency. Instead, using our equations - described in Chapter 4 - and consequently disposing of more variables, we can expect to have more frequencies. In this respect, results shown in Fig. 6.2 are very interesting.

These are also some of the reasons that made it necessary to export the analytical model, which stood as proof-of-concept, into a much more complex environment. In fact, the first two points can be easily neglected in CM in order to verify the applicability of the model. The lack of adjustable constant must be pointed out, as it provides the approach with general validity. When building the return map, it is useful to consider zero flame thickness as a first approximation. Assuming that fuel pressure at the inlet is constant, we can write:

$$dp_{inlet}(t - t_{convective}) = \zeta \cdot dQ_{exchanged}(t - \tau_p), \quad (5.4)$$

$$dp'_{inlet}(t - t_{convective}) = \bar{p}_{fuel} \cdot d \left(\frac{1}{1 - z_{inlet}} \right) (t - t_{convective}), \quad (5.5)$$

where the prefix d indicates a small quantity and ζ the acoustic coupling, which is a geometry dependent quantity. Together, the two previous expression lead to

$$dq^*(t - \tau_p) = d \left(\frac{1}{1 - z_{inlet}} \right) (t - t_{convective}). \quad (5.6)$$

Being $t_{convective}$ the time delay between the peak of perturbation of z_{inlet} and the heat release peak, it can be said that:

$$z_{flame}(t) = z_{inlet}(t - t_{convective}). \quad (5.7)$$

and consequently:

$$dq^*(t - \tau_p) = d\left(\frac{1}{1 - z_{flame}}\right)(t). \quad (5.8)$$

By considering the boundary conditions of no combustion ($q^* = 0$) when there is no air ($z_{flame} = 0$) and the case of no fuel ($z_{flame} = 1$), which implies that \bar{p}_{fuel} disappears and $q^* \rightarrow \infty$, it is possible to integrate equation (5.8) and obtain:

$$z_{n+1} = 1 - \frac{1}{1 + q_n^*}. \quad (5.9)$$

Knowing the value of q^* at time t , it is thus possible to predict the value of z_{flame} at $(t + \tau_p)$. Given this recursive relation, it is possible to investigate the behavior through time by knowing only the initial value of z_n and without numerical solution of equations given previously. In order to get back to a return map of the form of (5.3), the equations describing q^* are coupled with the initial assumption of null flame thickness and allows us to write:

$$q_n^* = \xi h(z_n), \quad (5.10)$$

Being ξ a Mach dependent quantity and knowing the relation between h and z . By combining equation (5.9) and (5.10), it is now possible to express the return map as:

$$z_{n+1} = 1 - \frac{1}{1 + \xi h(z_n)}. \quad (5.11)$$

Previous statements ensure that $z_{n+1} = 0$ for $z_n = 0$ or 1 and that z_{n+1} has one maximum between 0 and 1. Then, we observe its interaction with the fixed point equation (5.12).

$$z_{n+1} = z_n \quad (5.12)$$

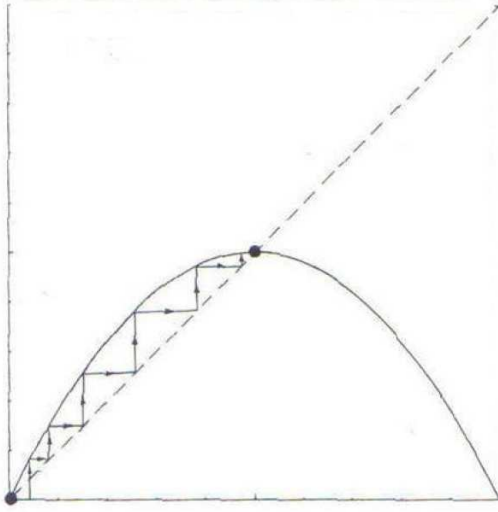


Figure 5.1: Equations (5.11) and (5.12) in the (z_n, z_{n+1}) plane

On the vertical axis of Fig. 5.1 is displayed z_{n+1} while z_n is displayed on the horizontal axis. The parabola-like curve is the return map expressed in (5.11) whilst the diagonal dashed line represent equation (5.12). Evolution of a system starting from a given state z_0 can be followed with the help of the arrowed line. The initial value of z is inserted into equation (5.11) and the result, found on the return map, is used back into (5.12) and so on. After a number of iterations, we get nearer and nearer to the fixed point $z_n = z_{work}$, the black dot at the intersection between the return map and the dashed line. The state z_{work} is often referred to as the attractor, while the stair-like arrowed path line is referred as the transient. Here, the depicted attractor is stable or, referring to our problem, humming-free because any perturbation $z_n \rightarrow z_n + dz_n$ produces a perturbation dz_{n+1} of z_{n+1} such that $|dz_{n+1}| < |dz_n|$. Stability condition can be summarized as follows:

$$\left| \left(\frac{dz_{n+1}}{z_n} \right)_{\xi_{critical}} \right| < 1 \quad (5.13)$$

Any system violating (5.13) should be considered unstable. Knowing that $\left| \left(\frac{dz_{n+1}}{z_n} \right) \right|$ is an increasing function of ξ and that same goes for ξ with Ma , we can consequently state that a system is stable when $Ma < Ma_{critical}$. In our application it is therefore possible, knowing z_{work} and $h(z_n)$, to find the value of $Ma_{critical}$. In the Fig. 5.2, a situation similar to the previous is plotted. Yet in this case, due to the different value of $\left| \left(\frac{dz_{n+1}}{z_n} \right) \right|$ - now almost 1 - it is possible to witness oscillations around the attractor before collapsing into it.

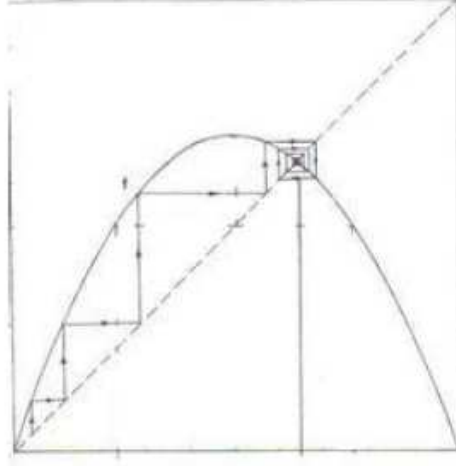


Figure 5.2: Another possible configuration of equations (5.11) and (5.12) in the (z_n, z_{n+1}) plane

As stated earlier, this is the case of zero flame thickness. When the flame thickness is considered, heat release equation becomes:

$$q_n^* = \xi h(z_n) - \frac{(\bar{p}\delta_f)\zeta}{4\bar{p}_{fuel}A_f(c-\bar{u})} \frac{dA_f}{dt} \quad (5.14)$$

By expressing $\frac{1}{A_f} \frac{dA_f}{dt}$ in terms of z and neglecting some flame-thickness-related quantities with the assumption of thin flame, it is possible to write a return map also for this case. In fact, it only differs from equation (5.11) for an additive term that includes the effects of flame motion. Given that the previous discussion regarding stability remains basically the same, these differences are of lesser important for the present thesis. Since no explicit analytical expressions for flame speed are available but for laminar flame, v_f is built as a function that depends on air molar fraction. Knowing that v_f has only one maximum when reaction is stoichiometric, which is $z_{stoichiometric} = 10/11$ for methane in air, and imposing vanishing flame speed for the limit cases of no air ($z = 0$) and no fuel ($z = 1$), the following equation is found:

$$v_f = v_{fM}h(z) = v_{fM} \frac{z^{1+C_1}(1-z)^{1+C_2}}{\left(\frac{1+C_1}{2 * C_1 + C_2}\right)^{1+C_1} \left(1 - \frac{1+C_1}{2 * C_1 + C_2}\right)^{1+C_2}}. \quad (5.15)$$

The maximum value of the flame speed v_{fM} is chosen case by case so that, when the flame speed is calculated in the reference condition z_{work} , the flame velocity is equal to the mean flow velocity.

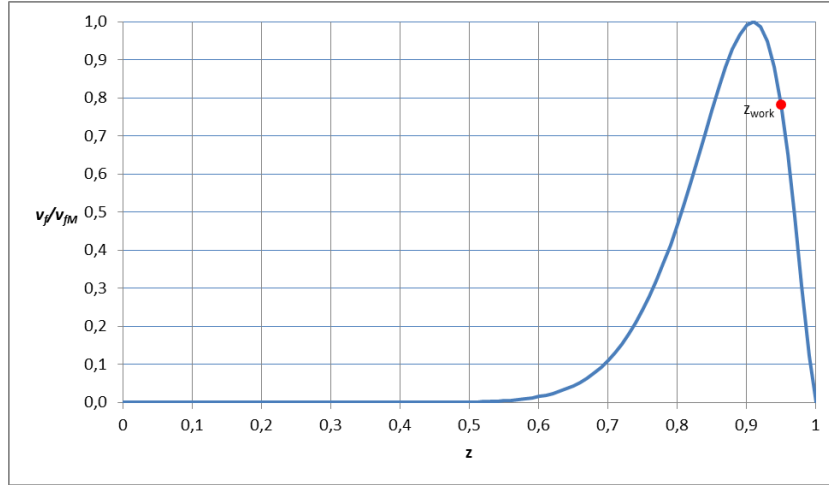


Figure 5.3: Flame velocity as a function of z

It is important to notice the high value in module of the first derivative right at $z_{stoichiometric}$. The flame shape is very important for two reasons. The first is related to the theory: as said before, the spatial distribution of heat release is very important when considering entropy waves. The second reason is related to our nonlinear heat release model: the flame shape is indirectly involved into calculations that determine the critical Mach number around which instability is triggered. Hence, this is the point where the artificial nature of our limit cycle mechanism is easier to spot: every simplification, for example assuming constant flame thickness, is a device to make it work faster. Furthermore, in the simulations using CM, the flame is often modeled as plane for the sake of computational effort but considered as an axisymmetric revolution surface. Its generator is a parabola, which rotates around an external axis. For example, the parameter I_{length} , which appears in the equation describing how the flame area varies over time, is estimated in the axisymmetric plane (r, x) , as:

$$I_{length} = 2\pi \int dr r \frac{\left(\frac{\partial f}{\partial r}\right)^2 \left(\frac{\partial^2 f}{\partial r^2}\right)}{\left[1 + \left(\frac{\partial f}{\partial r}\right)^2\right]}, \quad (5.16)$$

where f stands for the flame's profile in (r, x) . Disposing of an unperturbed and axisymmetric flame profile, I_{length} is calculated in the analytical model. Therefore, when considering a plane flame in CM, this very value is used despite not having a parabolic profile. Same goes for A_f . This simplification lowers the reliability of the 1D model. Indeed, the latter was utilized just to validate both the heat release model inside CM and the matching with the linearized balance equations.

Table 5.1: Heat release data from the analytical model

| Name | Value | Description |
|-----------------|------------|---|
| C_1 | 14.53 | Constant for flame velocity calculation |
| C_2 | 0.553 | Constant for flame velocity calculation |
| δ_f | 1 mm | Flame thickness |
| H | 49.6 MJ/kg | Higher heating value of methane |
| m_{air} | 0.029 kg | Molar mass of air |
| m_{fuel} | 0.016 kg | Molar mass of fuel |
| M_{air} | 20.4 kg/s | Air mass flow |
| M_{fuel} | 0.612 kg/s | Fuel mass flow - before the flame |
| $Ma_{critical}$ | 0.0071 | Critical Mach number |
| p_0 | 18.4 bar | Operating pressure |
| T_{inlet} | 661 K | Inlet temperature |
| z_{work} | 0.947 | Operating air molar fraction |

5.1 Including the heat release model inside our equations

Having roughly summarized the iterative mechanism, we can now go into detail for the heat release model which reads:

$$q^* = \frac{Q_{exchanged}}{(A_f \delta_f)}, \quad (5.17)$$

with $Q_{exchanged}$ the mechanical power supplied by the flame to the surrounding fluid:

$$Q_{exchanged} = Q_{combustion} - \frac{\bar{p} \delta_f}{\left(\frac{c_p}{c_v} - 1\right)} \frac{dA_f}{dt}. \quad (5.18)$$

The first term represents heat released by means of exothermic chemical reaction, while the second term models how heat exchanged varies depending on the flame motion. The first term will always be present, as it models power generated by combustion, whereas we will investigate effects of the second term with further simulations. We have:

$$Q_{combustion} = H A_f \rho Y v_f, \quad (5.19)$$

Which was the term expressed as air-molar-fraction-dependent in equation (5.14). The availability of pressure and temperature perturbations all over the geometry obtained by solving the linearized Euler equations may seem an excuse to estimate locally the

air molar fraction with the help of the Dalton law. It must be reminded that, even if real density, fuel mass fraction and velocity depend on local pressure and temperature perturbations, this analytical theory assume that, when calculating the heat release at the flame, the latter only depends on pressure perturbations at the inlet convected to the flame by (5.2). This is a macroscopic approximation whose misunderstanding, even with the intention of accurately describing the physic of the problem, would lead to different result. In fact, using our set of equations, it may be possible to describe heat release as a function of convectively advected perturbations, without using accessory equation (5.2), but this approach is not represented by the analytical theory we want to use. As far as initial conditions, pressure and air molar fraction are concerned, we have:

$$\bar{p}_{inlet} = \bar{p} = \bar{p}_{air} + \bar{p}_{fuel}, \quad (5.20)$$

$$\bar{z} = \bar{z}_{work} = \frac{\bar{p}_{air}}{\bar{p}_{air} + \bar{p}_{fuel}}, \quad (5.21)$$

$$\bar{n}_{air} = \frac{\bar{p}_{air}}{R_g \bar{T}_{inlet}}, \quad (5.22)$$

$$\bar{n}_{fuel} = \frac{\bar{p}_{fuel}}{R_g \bar{T}_{inlet}}. \quad (5.23)$$

At the inlet, the air molar fraction is estimated by the following equation:

$$\bar{z} = \frac{n_{air}}{n_{air} + n_{fuel}} = \frac{\frac{\bar{p}_{air} + p'}{R_g T}}{\frac{\bar{p}_{air} + p'}{R_g T} + \frac{\bar{p}_{fuel}}{R_g T}} = 1 - \frac{\bar{p}_{fuel}}{\bar{p}_{air} + \bar{p}_{fuel} + p'}. \quad (5.24)$$

The oscillating heat release is therefore linearized around working conditions. For example, considering only the first term on the right hand side of equation (5.18):

$$q' = \frac{H}{\delta_f} \rho(z) Y(z) v_f(z) - \frac{H}{\delta_f} \rho(\bar{z}) Y(\bar{z}) v_f(\bar{z}). \quad (5.25)$$

The most important of the three z -dependent terms is the flame velocity, therefore it will often be the only one we account for.

Chapter 6

Simulations

The first set of models is one-dimensional in order to understand the importance of each assumption. The geometry typically consists in: an inlet duct, a flame zone, and an outlet duct. In each section, we list the model's data. All values not listed in the following tables are to be intended using data listed in Tab. 5.1.

6.1 Model I

The first model is a replica of the geometry studied by the analytical model. In fact, an acoustically closed boundary condition is imposed after the flame. This assumption is not completely incorrect, because of the partial refraction caused by the temperature-related density change. Of course, such a boundary may never refract acoustic waves completely, but it give us a simple particular case to start with, whose results can be compared to the analytical theory.

Table 6.1: Model I data

| Name | Value |
|---------------------------|---|
| Boundary condition inlet | $u' = -\frac{p'}{10^5}$ (almost acoustically closed) |
| Boundary condition outlet | $u' = 0$ (acoustically closed) |
| Initial condition | $z = 0.9471$ and variable |
| $L_{inlet-flame}$ | 0.1 m |
| $L_{flame-outlet}$ | 0 m |
| $Ma_{critical}$ | variable |
| q' | $\frac{H}{\delta_f} \rho(\bar{z}) Y(\bar{z}) [v_f(z) - v_f(\bar{z})]$ |
| T_{outlet} | - |
| Temperature gradient | - |
| \bar{u}_{outlet} | - |
| μ_B | not considered |
| ϕ_{10} | considered |

Whatever inlet velocity we may take into consideration, geometry and mean temperature guarantee us that the following will always be true:

$$\frac{L_{inlet-flame}}{\bar{u}_{inlet}} + \frac{L_{inlet-flame}}{c_{c,inlet} - \bar{u}_{inlet}} > \frac{L_{inlet-flame}}{c_{c,inlet} + \bar{u}_{inlet}} + \frac{L_{inlet-flame}}{c_{c,inlet} - \bar{u}_{inlet}}, \quad (6.1)$$

which can be written, for a sufficiently small Mach number, as:

$$\frac{L_{inlet-flame}}{\bar{u}_{inlet}} > \frac{L_{inlet-flame}}{c_{c,inlet}}. \quad (6.2)$$

This means that pressure perturbations generated by the flame can travel from the inlet to the outlet and back several times before the effect of their first interaction with the inlet has reached the flame, consequently modifying heat release perturbations. Because of reflecting boundary conditions, the pressure perturbations at the inlet will keep building up until the first perturbed value of air molar friction gets to the flame. This immediately points out two important factors:

- the relation between the acoustic frequency and the convective mechanism frequency,
- the boundary conditions, which determines how much of the energy is bounced back inside the system and how much leaves it.

First, we assess the effect of the Mach number. This parameter may in fact be considered as a modifier of the first element of the list above, but its importance is

due to heat release model. In fact, the Mach number sets the mean flow velocity and, because of this, the maximum flame velocity (as seen in Chapter 5). The original analytical model stated that a stable limit cycle could be initiated with Mach number equal to the critical or higher. In Fig. 6.1 we observe pressure perturbation at the inlet for different simulations. Air molar fraction at the inlet follows the same behaviour, depending only on the pressure perturbation.

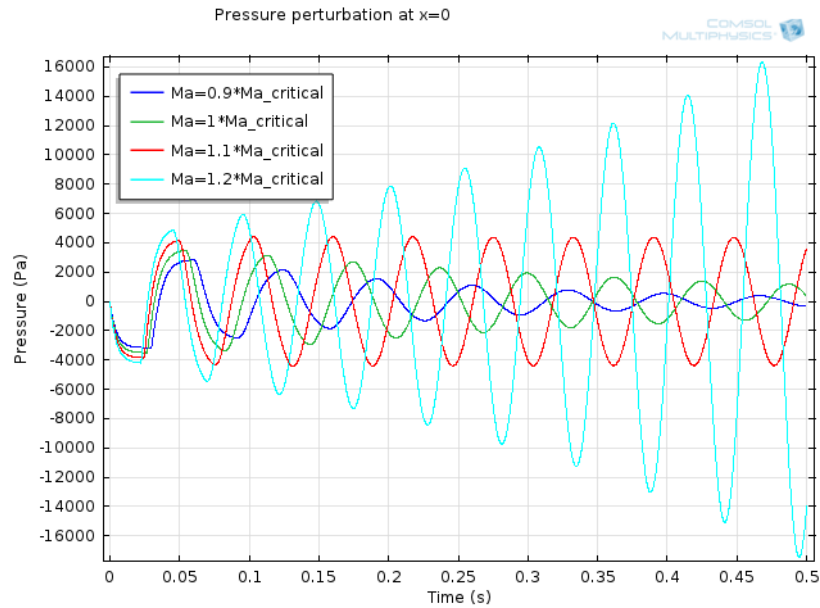


Figure 6.1: Pressure perturbation at the inlet for different mean flow velocity, Model I

We immediately note that a stable limit cycle is reached for Ma slightly larger than critical. This difference from the analytical model can be due to the acoustic impedance at the inlet, to the presence of viscous dissipation and to the fact that we are now considering only air and not an air-gas mixture as a first approximation. This allows sound speed to be slightly higher than the one considered by the analytical model, consequently modifying the value of critical Mach number. According to the analytical model, stable limit cycles should be reached even when considering Mach numbers higher than the critical. Observing Fig. 6.1 we cannot tell if the light blue simulation has reached a stable cycle. Therefore, we run a longer simulation for this case to confirm complete accordance with the analytical model.

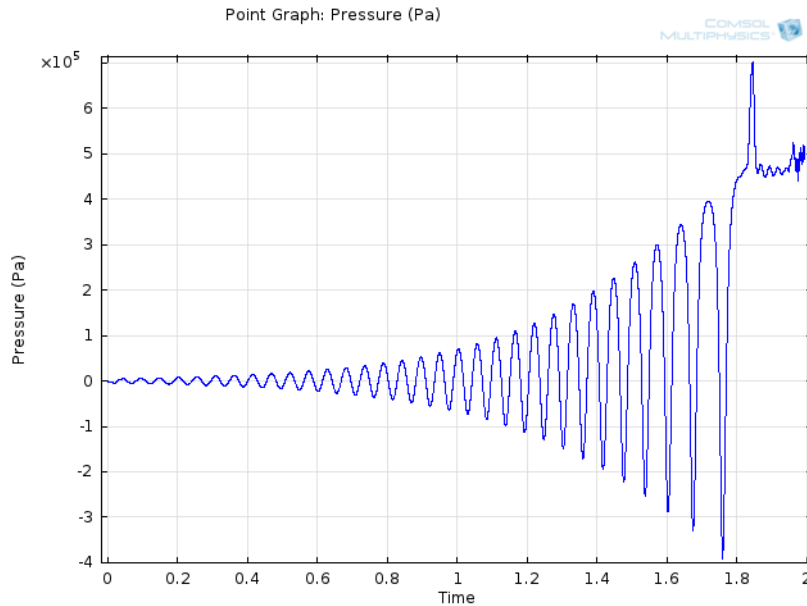


Figure 6.2: Pressure perturbation at the inlet when $Ma = 1.2 \cdot Ma_{critical}$

The high values reached by pressure perturbation in Fig. 6.2 immediately suggest us that this results should be considered with caution. First of all, we must remind that the analytical theory was confirmed for values around Mach critical, which means translated to our simulations- for values around 1.1 times the critical Mach. Furthermore, a time of 2 seconds is way beyond humming transients and so we should have stopped our investigations way before. Nonetheless, this simulation allows us to observe an interesting peak at 1.8 seconds. This peak, and the following high-frequency plateau, may in fact be the evidence of a two-frequency limit cycle. The original analytical approach, being in one variable, could not include this possibility, which is in fact possible with our set of equations. Ultimately, this last simulation does not give us further information about the correctness of implementation of the analytical model within COMSOL, but it allows us to start considering how the two affect each other. On the basis of results obtained, we start investigating how each parameter - such as different geometries, initial and boundary conditions and mean values - change the system's behavior. We start on the geometry just seen, only varying the inlet condition.

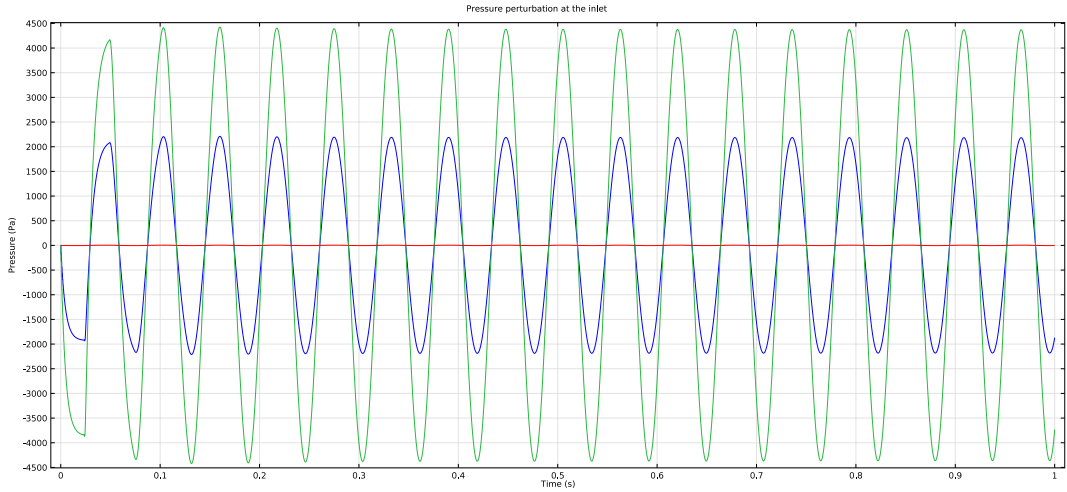


Figure 6.3: Pressure perturbation at the inlet with $Ma = 1.1 \cdot Ma_{critical}$. Green line: $z_0 = 0.9471$, blue line: $z_0 = 0.94705$, red line: $z_0 = 0.9470001$

Fig. 6.3 allows us to evaluate the dependence of the system from the initial condition: comparing the three simulations, we immediately note that halving the initial air molar fraction halves the amplitude of the limit cycle. Indeed, the amplitude of the limit cycle decreases as the initial air molar fraction gets closer to its work condition. This result is in agreement with on-duty behaviour of typical gas turbines: by increasing the fuel quantity, humming is suppressed.

6.2 Model II

On the basis of results of Model I, the mean flow velocity is slightly higher than the one required by the analytical model to initiate a limit cycle.

Table 6.2: Model II data

| Name | Value |
|---------------------------|---|
| Boundary condition inlet | $u' = 0$ (acoustically closed) |
| Boundary condition outlet | $u' = 0$ (acoustically closed) |
| Initial condition | $z = 0.9471$ |
| $L_{inlet-flame}$ | 0.1 m |
| $L_{flame-outlet}$ | 9.4 m |
| $Ma_{critical}$ | $1.1 \cdot Ma_{critical}$ |
| q' | $\frac{H}{\delta_f} \rho(\bar{z}) Y(\bar{z}) [v_f(z) - v_f(\bar{z})]$ |
| T_{outlet} | 1200 K |
| Temperature gradient | step-like, after the flame |
| \bar{u}_{outlet} | $3 \cdot \bar{u}_{inlet}$ |
| μ_B | not considered |
| ϕ_{10} | not considered |

We immediately note that, for this system:

$$\frac{L_{inlet-flame}}{\bar{u}_{inlet}} < \frac{2L_{inlet-flame}}{c_{c,outlet}}. \quad (6.3)$$

The analytical model only cared for the interaction between the inlet and the flame, without considering that the forward-directed pressure perturbation produced by the oscillating heat release would eventually be bounced back with a certain delay, perturbing the inlet differently through time. Inequality (6.3) shows that, here, the convective mechanism happens faster, reaching the flame before all the energy produced by it reaches the inlet. We can easily estimate frequencies. The following figures show the pressure perturbation at the outlet and its frequency spectrum.

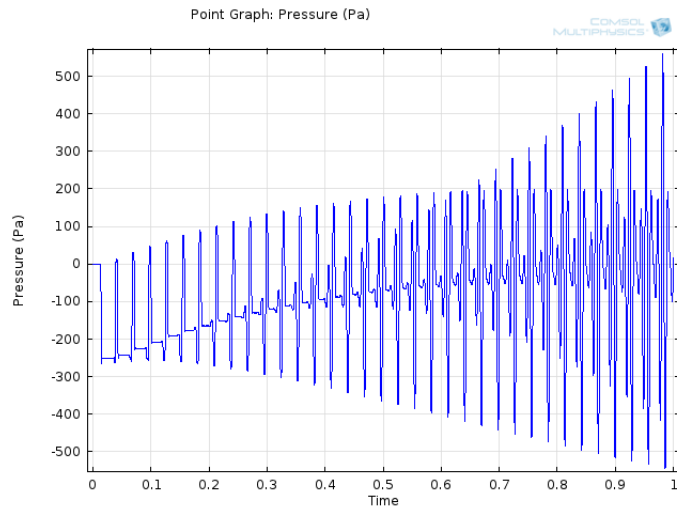


Figure 6.4: Pressure perturbation at the outlet over time [s], Model II

The oscillations seems to grow without bounds. However, for this simulation and the following, it is not very interesting to understand their upcoming behaviour. The first reason is that we are now facing particular cases: without a precise interest, the importance of a qualitative evaluation of the phenomenon becomes of main relevance. The second reason is that, for the phenomenon we are analyzing, a time of one second or more is not necessary.

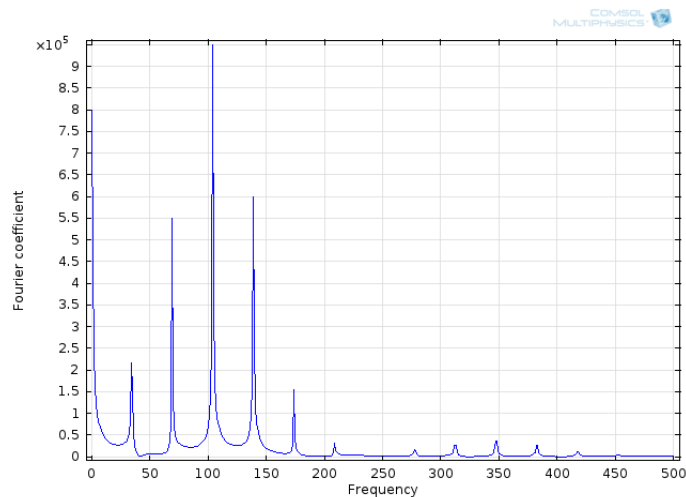


Figure 6.5: Frequency spectrum of the pressure perturbation signal at the outlet over time [s], Model II

Frequency spectrum shows similar peaks in all resonant frequencies, so we can assume that, in this configuration, each natural frequency is excited by the heat release.

Therefore, the Rayleigh criterion can be evaluated as expressed by (1.1). Even without considering the first step caused by the initial conditions, the Rayleigh criterion is in fact satisfied.

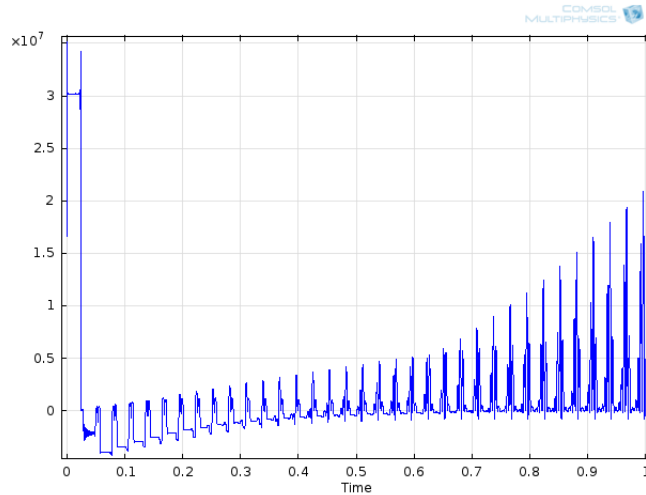


Figure 6.6: (p', q') integrated over the flame length; on the x-axis, time in seconds

This model and the following show the importance of knowing with precision the geometry, the mean temperature field and especially the acoustic impedance at both ends. In fact, acoustic impedance usually change with frequency, modifying energy loss through the boundaries according to pressure perturbations. Knowing the acoustic impedances is consequently of fundamental importance when looking for stable oscillations. The verification of the satisfaction of the Rayleigh criterion should be done case by case and is here purposed as an example.

6.3 Model III

This model is identical to the previous except for the length that separates the flame from the inlet.

Table 6.3: Model III data

| Name | Value |
|---------------------------|---|
| Boundary condition inlet | $u' = 0$ (acoustically closed) |
| Boundary condition outlet | $u' = 0$ (acoustically closed) |
| Initial condition | $z = 0.9471$ |
| $L_{inlet-flame}$ | 0.1 m |
| $L_{flame-outlet}$ | 6.1 m |
| $Ma_{critical}$ | $1.1 \cdot Ma_{critical}$ |
| q' | $\frac{H}{\delta_f} \rho(\bar{z}) Y(\bar{z}) [v_f(z) - v_f(\bar{z})]$ |
| T_{outlet} | 1200 K |
| Temperature gradient | step-like, after the flame |
| \bar{u}_{outlet} | $3 \cdot \bar{u}_{inlet}$ |
| μ_B | not considered |
| ϕ_{10} | not considered |

Thus, we observe:

$$\frac{L_{inlet-flame}}{\bar{u}_{inlet}} > \frac{2L_{inlet-flame}}{c_{c,outlet}}. \quad (6.4)$$

The results are very different from the previous: the next two figures show pressure perturbation signal at the outlet and its frequency spectrum.

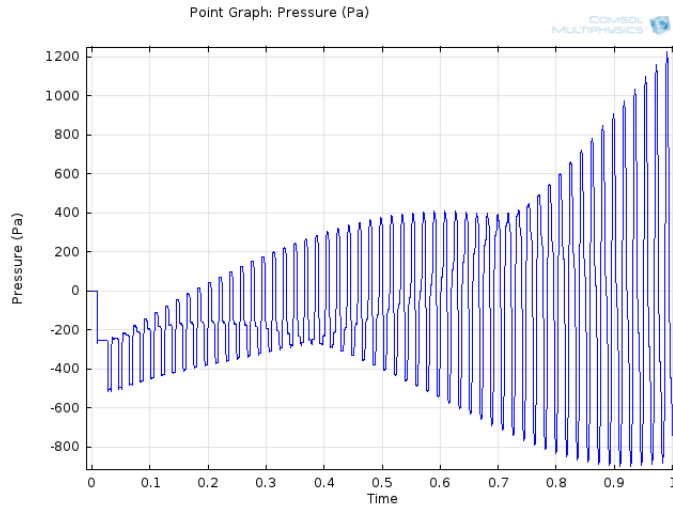


Figure 6.7: Pressure perturbation at the outlet over time [s], Model III

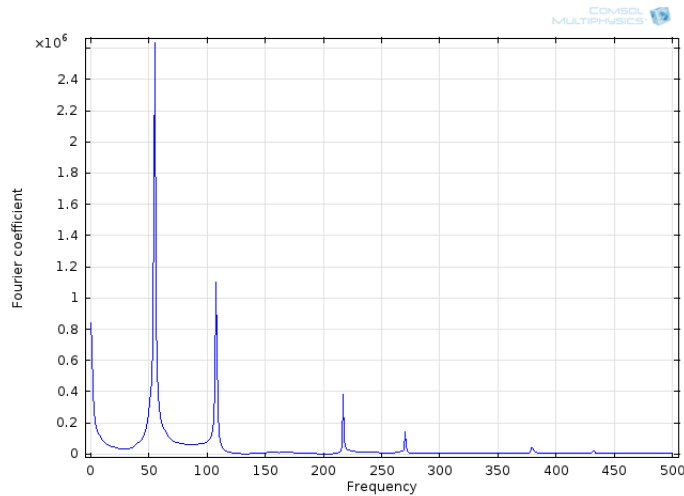


Figure 6.8: Frequency spectrum of the pressure perturbation signal at the outlet over time [s], Model III

In Fig. 6.8 we can observe how the first fundamental frequency of the flame-outlet duct stands out, which was not the case in Model II (Fig. 6.5), where all fundamental frequencies had a peak of almost the same height. Of course, this different interaction between energy release and natural frequencies strongly depends also on the boundary conditions and is here pointed out only for qualitative consideration, with the aim of showing interactions between heat release and geometry.

6.4 3D Models

In order to test our model in a realistic environment, we decided also to make some tests in a three-dimensional geometry. The best validation for this model would have been AE's test rig in Sesta, but the availability of accurate temperature, velocity and reaction rate fields obtained with Fluent simulations, induced us to consider the geometry of the combustion chamber of AE's gas turbine 64.3a. Despite having such useful and complete information, we still had to make some approximations: first, we had to simplify the geometry in order to have the best balance between modeling a meaningful domain and reducing the computational time. At the very beginning of this study we considered modeling only one sector out of the 24 that compose the combustion chamber. The difficulty of expressing the boundary conditions appropriately and the consequent impossibility to analyze meaningfully the obtained results, convinced us to consider the full combustion chamber. Even by doing so, we still had to face the problem of the unknown acoustic boundary conditions at the inlet and at the outlet. In this phase of our study, to reduce the computational load of the simulation, we decided not to include the plenum surrounding the combustion chamber. Secondly, we had to

face a new but fundamental issue: instead of the 1 mm wide flame we were used to until now we had a distributed flame shape with different reaction rates. As a first approximation, we decided to normalize the given reaction rate and to simultaneously introduce a scale factor to reduce the unforeseen effect of a distributed flame. The idea is to modify the entity of this scale factor through time by conducting simulations on the test rig mentioned before. Since then, the meaning of these simulations is more to understand if an oscillation can be realized rather than evaluating its actual amplitude. The geometry considered is shown in Fig. 6.9, the mesh consist of 64101 elements. The physical conditions such as temperature and velocity field are provided by a CFD analysis of the single sector and are imported to CM with the help of a FORTRAN code. All the boundary conditions are set as acoustically closed ends: this is a strong simplification when considering the inlet and the outlet surfaces, but can acceptably describe all the others. This simulation rapidly reaches non-physical values of the pressure perturbation, but its behaviour is nevertheless interesting as it allows us to have a better understanding of the differences between this kind of simulation and the previous 1D simulations. More results are of course needed to provide full confidence in the tool developed, and this is the object of future work.

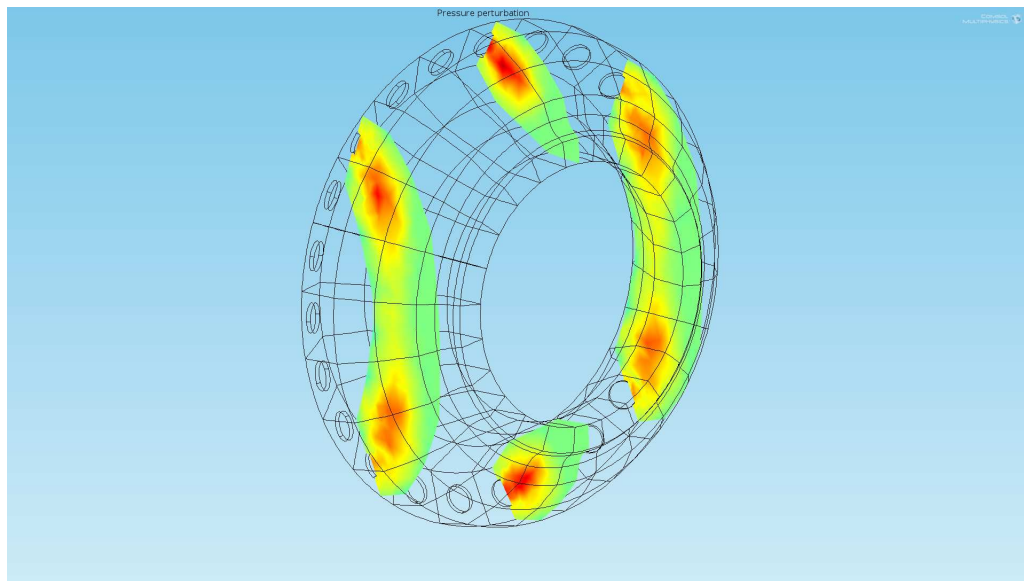


Figure 6.9: Pressure perturbation inside the annular combustion chamber after a time $t = 10^{-4}[s]$ from the beginning of the simulation

Chapter 7

Conclusions and future developments

As stated at the beginning of this thesis, the humming phenomena and its phenomenology are still objects of intense research activities. In this thesis, we tried both to refine academic approaches and to introduce new mechanisms inside the environment of COMSOL Multiphysics. The two have proved to be closely linked: the mean flow studied in the first steps of this thesis is in fact one of the most important triggers of the heat release model eventually developed. Now, disposing of our own set of linearized equations and respective dependent variables, we may also take into consideration the possibility of modelling the heat release in a more physical fashion, without the help of accessory equations to describe stoichiometry convection. This is a theoretical, long-term future development that may deepen the meaning of the present approximations while making full use of the new physics we have developed within the computational environment employed. In the meantime, our work is a simple but ready-to-use tool that may be useful to investigate the possibility of the onset of a limit cycle in complex geometries of known velocity and temperature field, flame shape and acoustic boundary conditions. Consequently, it obviously needs to be closely linked with CFD and measurements data. The present approach may ultimately be used, once validated, to plot the bifurcation map of a given system evaluating its sensitivity to different parameters - not just Mach number, initial condition or geometry - in order to estimate predictively whether the system is prone to humming or not.

Bibliography

- [1] Hatout, J.P., *Thermoacoustic Instability. Fundamentals and Modeling in Combustion*, 1999.
- [2] Farhat, S. A. and Al-Taleb, M. K., *Combustion Oscillation Diagnostics in a Gas Turbine Using an Acoustic Emission*. Jordan Journal of Mechanical and Industrial Engineering, Vol. 4, pag. 352–357 2010.
- [3] Rayleigh, J. W. S. *The Explanation of Certain Acoustical Phenomena*. Nature, vol. 18, pag. 319-321 1878.
- [4] Polifke, W. *Combustion Instabilities*. VKI Lecture Series "Advances in Acoustics and Applications", Brussels, Belgium, 2004.
- [5] Lieuwen, T. C. and Cho, J. H. *Modelling the Response of Premixed Flames Due to Mixture Ratio Perturbations*. GE2003-38089, ASME Turbo Expo Atlanta, Georgia, U.S.A, 2003.
- [6] Dowling, A. P. *The calculation of thermoacoustic oscillation*. Journal of Sound and Vibration, Vol. 180, num. 4, pag. 557-581, 1995.
- [7] Nicoud, F. ; Wieczorek, K. *About the zero Mach assumption in the calculation of thermoacoustic instabilities*. International journal of spray and combustion dynamics, Vol.1, pag. 67-112, 2009.
- [8] Ing. Fabio Valle, Ansaldo Energia, *Modello a parametri concentrati per la simulazione dello humming - T08321VR1000*.
- [9] Campa, G. *Calcolo acustico camera anulare attuale AE*. 2010.
- [10] Dowling, A. P. ; Storw, S. R. *Acoustic Analysis of Gas Turbine Combustors* Journal of Propulsion and Power, 19 (5), pag. 751-765, 2003.
- [11] Pankiewitz, C.; Sattelmayer, T. *Time Domain Simulation of Combustion Instabilities in Annular Combustors* Journal of Engineering for Gas Turbines and Power, Vol. 123, n. 3, pag. 677-685, 2003.
- [12] *COMSOL Multiphysics: Deriving the Weak Form*

Appendix I

Acoustic and entropy waves are different ways of propagation for perturbations inside a moving fluid. Their dispersion relations $\omega = \omega(\mathbf{k})$, are the limit cases, respectively for zero velocity and zero sound speed, of the roots $\omega = \mathbf{k} \cdot \mathbf{u} \pm |\mathbf{k}| \cdot c$ of the dispersion relation valid in a moving fluid. Here, \mathbf{k} is the wave vector and ω is the angular frequency. For zero velocity ($\mathbf{u} = 0$), different signs in ω indicate different propagation direction. Dependency on $|\mathbf{k}|$ implies symmetry with respect to propagation direction for uniform c . Propagation is driven by pressure gradients. For zero sound speed ($c = 0$), the wave is stationary in the fluid's coordinate system, therefore perturbation moves with the fluid.

Acknowledgements

I would like to express my gratitude for the professional and personal support provided by Dr. Ezio Cosatto and Dr. Andrea Di Vita.

My appreciation also extend to Prof. Alessandro Bottaro, who made this experience possible and has always supported its progress.

This thesis would have never been possible without the continuous and sympathetic support of the people composing my life: they know who they are.